Sensors & Transducers, Vol. 237, Issue 9-10, September-October 2019, pp. 95-102

www.sensorsportal.com

Sensors & Transducers

Published by IFSA Publishing, S. L., 2019
http://www.sensorsportal.com

Micro-calorimetric Flow Rate Measurement Device for Microfluidic Applications

Bilel Neji
College of Engineering and Technology, American University of the Middle East, Kuwait
Tel.: +965 22251400, fax: +965 26548484
E-mail: bilel.neji@aum.edu.kw

Received: 30 August 2019 /Accepted: 27 September 2019 /Published: 30 November 2019

Abstract: With the recent advances in biology and medical fields, nano and micro sensors became essential for accurate measurements and diagnosis. Miniaturization of such critical devices has become essential to operate in micro scale circuits, including microfluidic devices that can be used for applications including preclinical diagnosis, drug monitoring and delivery, and lab on chip devices. Several techniques have been used to measure fluid flow rate. These techniques can be classified as thermal and non-thermal. This research focuses on calorimetric flow rate sensors, which is a sub-type of thermal flow rate sensors. This paper presents the design, microfabrication and characterization of a micro-calorimetric flow rate sensor. The device is capable of measuring fluid flow rates starting between 10 $\mu L/h$ and 1 mL/h. The sensing part of the device, excluding the power supply, measures 1 mm by 4 mm. The channel width and height are both equal to 100 μm. Experiment results show that measured output voltages ranging from 0.1 mV to 0.28 mV, correspond to flow rates between 100 $\mu L/h$ and 700 $\mu L/h$. The device flow rate measurement error is around 2 $\mu L/h$, and the device response time is less than 3 seconds.

Keywords: Micro-calorimetric measurement, Microfluidics, Fluid flow rate, Heat transfer, Temperature sensing, Microfabrication.

1. Introduction

Flow rate sensors have been widely used in biomedical engineering and research development. Flow rate sensors are key components used in a wide range of applications, including drug delivery, blood flow monitoring, and Lab on a Chip devices [1-4]. Several techniques have been used to measure fluid flow rate. These techniques can be classified as thermal and non-thermal. Non-thermal techniques include mechanical flow sensors and Coriolis mass flow meters. Mechanical flow sensors are considered as one of the most important groups of non-thermal flow measurement techniques. Fluid flow is usually laminar in microfluidics channels. Therefore, calculation rules of drag force on the channel walls and the pressure drop in the direction of the fluid flow are known. Both drag and pressure drop are directly proportional to the velocity of the fluid flow. The authors in [5] stated that using piezo-resistive transducers and/or integrated pressure sensors, the flow velocity can be deduced and thus the flow rate in the sensor can be determined. On the other hand, the use of mass flow meters in microfluidics is growing as the technology is getting improved for microscale flows. In a mass flow meter operating on the "Coriolis principle", the fluid flows on a vibrating channel. The Coriolis force acting on the moving fluid will affect the frequency, phase shift or amplitude of the initial vibration proportionally to the mass flow rate. The

advantage of using Coriolis mass flow meter is that the measured flow rate and the properties of the liquid are totally independent. In addition, there is no need for calibration for such kind of sensors to measure or monitor gas or oil flows. One of the disadvantages of this technique is its relatively high cost. In addition, the small inner diameter of the fluidic path might not be suitable for biological experiments. Other non-thermal techniques to measure flow rate in microfluidics are using optics technology. The authors in [6] presented a flow sensing method based on the measurement of electrical admittance of conducting liquid. This technique is used to measure flow rates below $1\ nl/s$. Micro Particle Image Velocimetry (micro PIV) has been used as an optical method for micro flows analysis due to its capability of measuring other entities including velocity flow field. One of the disadvantages of micro PIV is its high cost [7]. Video microscopy is another popular optical flow measurement method that was proposed in [8]. This method employs the displacement of a liquid column in a microchannel observed through a microscope to determine the flow rate. The fluid flow rate is calculated from the time in which the liquid column travels over a fixed distance [8]. In addition to the mentioned technologies, several other non-thermal solutions for flow rate measurement have been proposed by researchers in the field. These techniques include acoustics and electrochemical phenomena.

The research presented in this paper focuses on thermal based sensors, with no moving parts. Thermal flow sensors have several advantages such as their small size, low power consumption, and high sensitivity at different flow rates. Several thermal flow sensing methods have been employed in the field, including hot-wire and hot-film, time of flight, and calorimetric method, which is mainly based on measuring the difference between the fluid's initial temperature and its temperature after being in contact with a heating element [9-10]. In this paper, a calorimetric microfabricated thermal flow rate sensor is proposed for microfluidic applications. Experimental results demonstrate that an applied heat generated by an applied voltage V_{in} to the heating element can be transduced into an electrical signal V_{out}, measured at the outlet temperature sensor, to determine the fluid flow rate.

2. Thermal Flow Sensors Overview

The working principle of thermal flow rate sensors is based on the heat transfer between the heating element, also called heater, and temperature sensors through the microfluidic channel. The output temperature is proportional to the flow rate change. There are different forms of thermal flow sensors, and the most known ones are hot-wire and hot-film, time-of-flight, and calorimetric techniques. Hot-wire and hot-film method relies on the measurement of the heat transfer from the heating element to the fluid: The sensor uses a resistive wire in the case of hot-wire technique, and a resistive thin film is used in the case of hot-film technique. When the liquid flows over the sensor, carrying some of the heat from the heating element, the temperature sensor resistance changes accordingly, and that change corresponds to a specific flow rate change. On the other hand, time-of-flight technique is based on the concept of measuring the transition time of a thermal pulse generated by the heating element to reach the temperature sensing element. The measured time is proportional to the properties of the fluid, including its thermal conductivity and its diffusivity, the average velocity of the flow, and the distance between the heater and the temperature sensor. Calorimetric sensors use a heating element and two temperature sensors: one at the inlet of the channel, and the other at the outlet of the channel. The outlet temperature sensor detects the thermal profile caused by the liquid flowing by. The difference in the thermal profile will be proportional to the liquid flow rate [11]. The flow direction can be deduced from the difference between the two temperature sensors' measurement. It should be mentioned that the type of the fluid and its proprieties have to be well known for an accurate measurement of the flow rate. The presented thermal flow rate measurement techniques are illustrated in the diagrams of Fig. 1.

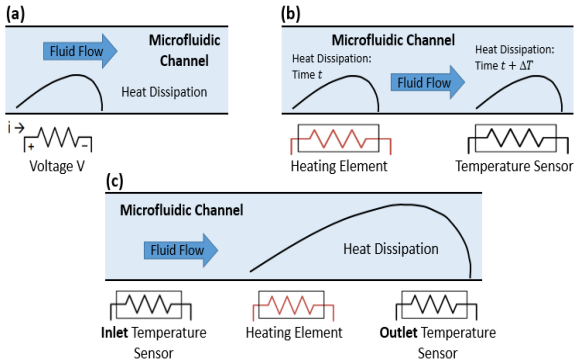

Fig. 1. (a) Hot-wire and thin-film method; (b) Time of flight method; (c) Calorimetric method [9].

Now a day, the miniaturization of flow rate sensors based on the described techniques has become essential in the field of micro and nano technology. Thermal flow sensors have a great utility in industrial, biomedical and research fields for monitoring and control operations [12]. Several research projects have been focusing on micro systems development that can accurately measure fluid flow rates. A MEMS based flexible flow sensor for online monitoring of body fluid and blood is presented by the authors in [13]. The authors analyzed the effect of different geometries of the resistive heating element placed on a substrate of different materials. Thermal flow rate sensors have also been used to monitor the accuracy and life time of micro pumps. Drug supply micro pumps have been widely used as a medical treatment of diabetes to supply insulin. These pumps have to be small and

accurate. The research in [14] presents an osmotic pressure pump, and a magnetic-driven pump, using miniaturized actuators based on a semi-permeable membrane and a magnet. In the recent years, with the research and technology advances, it became possible to fabricate complete systems combining a variety of micro sensors. PDMS (Polydimethylsiloxane) has been widely used to create microfluidic systems made of different modules that are either microfabricated using lithography and metal deposition, or using advanced 3D printing [15-16].

3. Flow Rate Micro Sensor Design

3.1. Flow Rate Sensor Principle

The proposed thermal flow rate sensor uses the calorimetric technique at the micro scale. Energy cannot be created nor destroyed; it can only be converted from one form to the other. The designed sensor uses this concept to transduce an applied voltage into thermal energy, to be transferred to a fluid in contact with a heating element. The fluid will carry the heat and transfer it to the outlet temperature sensor. An inlet temperature sensor is used to determine the fluid's initial temperature. Each measured temperature raise at a specific applied voltage will correspond to a specific flow rate of the fluid. A block diagram of the proposed flow rate sensor is shown in Fig. 2.

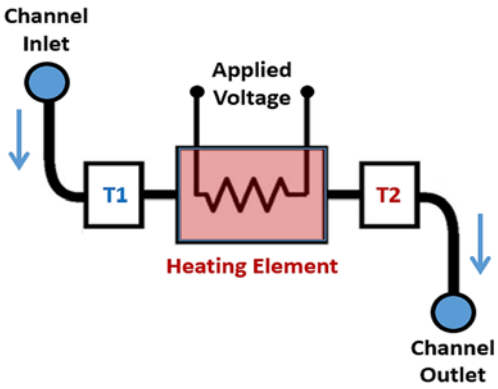

Fig. 2. Flow rate sensor block diagram.

The heating element is location between the two temperature sensors. $T1$ corresponds to the fluid initial temperature before contacting the heating element, and $T2$ is the fluid's temperature after being heated.

3.2. Sensor Simulation

The simulation of the thermal flow rate sensor has been performed using two different fluids: oil, and water. The proposed design of the thermal flow rate is shown in Fig. 3. Different structures with different dimension have been simulated.

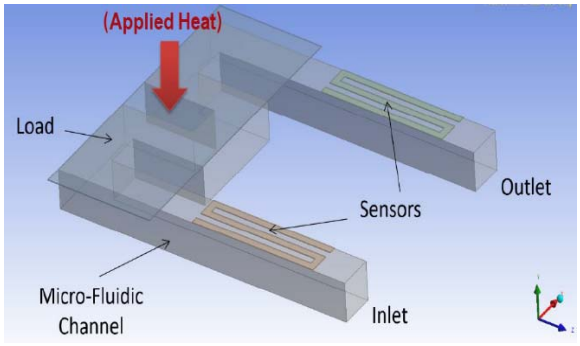

Fig. 3. Proposed micro calorimeter design for simulation.

The simulation results confirm the working principle of the calorimetric method for flow rate sensing. This can be illustrated in Fig 4.

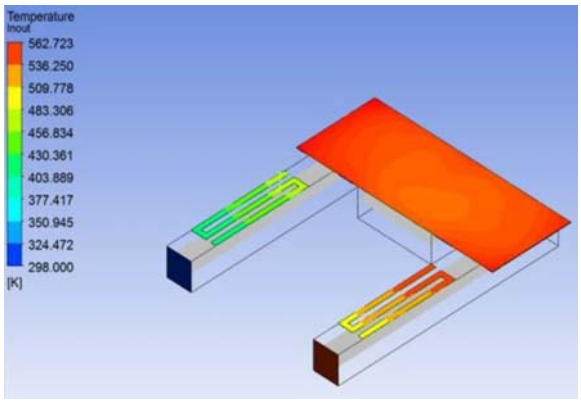

Fig. 4. Example of temperature profile of the heating element and the inlet & outlet sensors.

The simulation results in Table 1. Correspond to a heating element structure that has the following specifications: Thickness is 1 μm; length is 160 μm, and width is 400 μm. The used flow rate is 1000 $\mu l/h$ and the applied power to the load is equal to 100 μW.

Table 1. Temperature variation between the input sensor and output sensor using oil then water as fluids.

	Inlet Sensor's $T1$	**Outlet Sensor's $T2$**	**ΔT (oK)**
Oil	352	366	14
Water	298	320	22

It can be concluded that water is better than oil for heat transferring from the heating element to the outlet temperature sensor. Water transfers almost double the amount of heat transferred by oil. Therefore, water will be used to simulate the real prototype.

3.3. Flow Rate Sensor Physical Design

The physical design of the microfabricated flow rate sensor is shown in Fig. 5(a). It consists of a microfluidic channel with a serpentine structure

bonded on the heating element to be used to transfer the heat to the fluid. PDMS is used to make the microfluidic channels. The heat is generated by the applied voltage V_{in}, the equivalent of an applied power P_a. The heating element is a thin film made of tantalum nitride. Tantalum nitride has been chosen due to its low temperature coefficient of resistance (TCR). Low TCR is critical for the heating element to maintain uniform resistance in the large range of operating temperatures. The temperature sensors are made of platinum due to its linearity and relatively high TCR [17]. All metals and PDMS are deposited on a glass substrate. Glass has a very low thermal conductivity, which is 100 times smaller than that of silicon. Lower thermal conductivity is required to limit unwanted heat loss to the substrate and the surroundings. Fig. 5(b) presents a zoom-in of the microfluidic channel, the temperature sensors and the heating element. The heating element is shown in red; the microfluidic channel is in blue; and the inlet & outlet temperatures sensors and the coplanar waveguide, used to transfer the applied voltage to the heating element, are in grey.

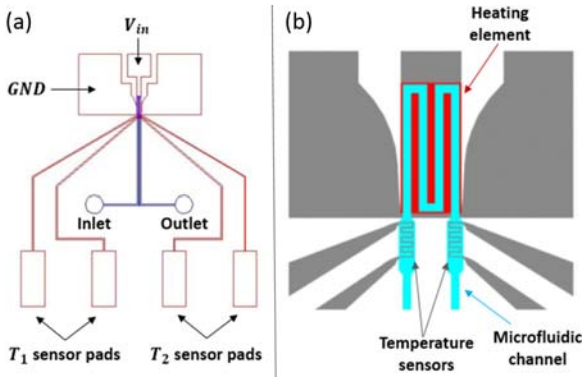

Fig. 5. (a) Design of the proposed flow rate sensor; (b) Zoom-in of the designed heating element and temperature sensors.

4. Thermal Flow Sensor Microfabrication

4.1. Fabrication Process

The proposed flow rate sensor is microfabricated in a 1000 class cleanroom environment.

Microchannel Fabrication:

In the process of microuidics fabrication, a mold is first produced. The mold is prepared on a silicon substrate and using the concept of photolithography to get the required design onto the mold. Then, soft lithography is employed to make the PDMS fluidic layer. The general procedures used in single-depth photolithography can be described In Fig. 6.

Since microfluidic devices work in small scale dimension, the surface contamination on the substrate must be cleaned to ensure perfect operation of the PDMS device. A 3-inch silicon wafer is first treated with hydrofluoric acid for 5 minutes to remove its silicon dioxide layer. Then acetone, methanol and DI water are used one by one to remove the dirt particles on the surface. Lastly, after drying with nitrogen gas, the silicon wafer is ready for spin coating.

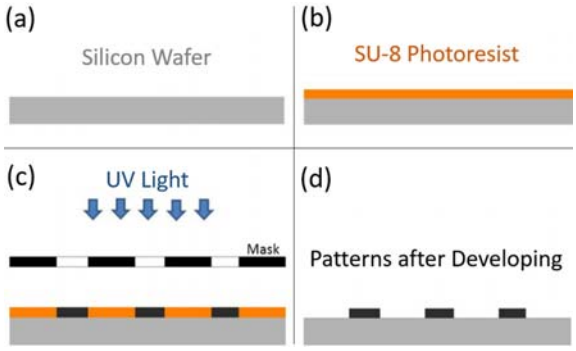

Fig. 6. General process for single-depth photolithography: (a) Substrate preparation; (b) Spin coating; (c) UV exposure; (d) Development.

For microfluidic mold fabrication, a negative photoresist SU-8 is usually used for this purpose. Three different types of SU-8 were applied in our case. For the 35 μm thickness lower layer, SU-8 2050 was placed on the substrate and then rotated at 4500 rpm for 30 seconds. The substrate is then placed on a hot plate for pre bake. The bake time is 1 minute for 65 $°C$ and 5 minutes for 95 $°C$. The purpose of pre bake is to evaporate excess coating solvent and harden the photoresist. UV exposure is a process of transferring pattern from the mask to photoresist. We can selectively remove parts of photoresist to get a desirable mold after its UV exposure under a predefined mask. For the negative photoresist SU-8, the area exposed to the UV light would become harder and insoluble within developer. Post bake is used to harden the photoresist. The wafer is baked at 65 $°C$ for 1 minute and at 95 $°C$ for 5 minutes. Lastly, the wafer is dipped into the SU-8 developer for 4-5 minutes. The part exposed to the UV light remains while the other part gets dissolved. Soft lithography refers to process that transferring pattern from SU-8 model to PDMS. PDMS is a moldable, biocompatible and optically transparent elastomeric polymer which has been widely used in microfluidic device fabrication. The process of soft lithography is shown in Fig. 7.

The SU-8 model is first treated with hexamethyldisilazane (HDMS), a release agent which works well for stripping of PDMS from the mold. Sylgard 184 silicone elastomer base and Sylgard 184 silicone elastomer curing agent are prepared for making PDMS. They are mixed with a ratio of 10:1.

Then the mixture is kept in the vacuum oven for degassing to get rid of air bubbles. The mixture is casted on the SU-8 model and cured at 60$°C$ until the PDMS is fully hardened. Lastly, the PDMS is peeled off from the SU-8 mold. Inlets and outlets are punched with blunt needle.

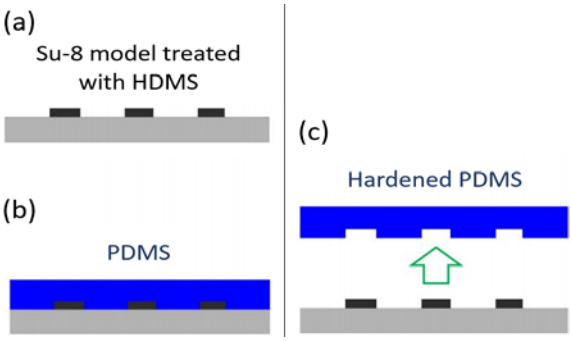

Fig. 7. Process of soft lithography: (a) SU-8 model preparation; (b) Pouring the PDMS over the model and curing; (c) Peeling off the PDMS.

Metal Patterns Deposition:

Photolithography and e-beam evaporation are employed for tantalum nitride and platinum deposition on glass.

The E-beam evaporation machine is used to deposit aluminum for the temperature sensors and connection lines. It is also used to deposit several other metals, such as silver and gold, for optimization and test purposes. Electron beam evaporation technique is based in the heat produced by high energy electron beam bombardment on the material to be deposited [18, 19]. Emitted electrons from the electron source are accelerated towards an anode by a high difference of potential in the order of kilo volts. The crucible itself or a near perforated disc can act as the anode. A magnetic field is used to bend the electron trajectory (Fig. 8).

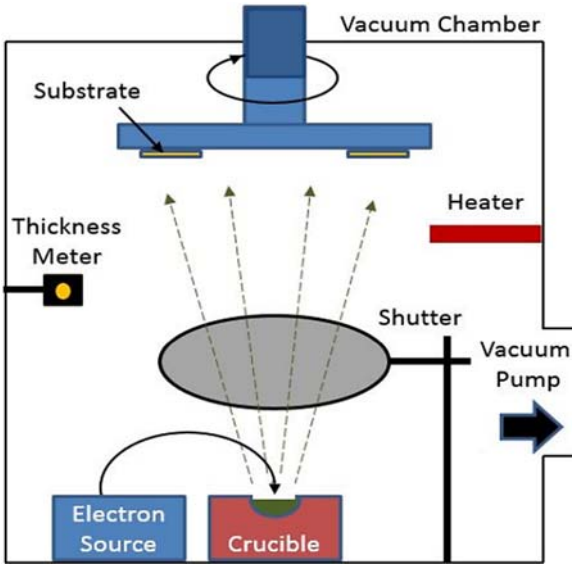

Fig. 8. Simplified Electron beam evaporation system diagram.

The electron beam can be precisely controlled using electric and magnetic fields. It can be scanned at high speed within a specified area, and the beam can be irradiated with the optimal electric density for the evaporant material. An ultra-high vacuum pump is used to keep the chamber pressure around 10^{-6} Pa.

4.2. Microfabricated Sensor

It should be noted that different devices are fabricated while optimizing several parameters of the design, including the width of the sensors' patterns, the spacing between the patterns, the microfluidic channel width, and the minimum spacing between channels. In addition, metal deposition process is optimized by varying several parameters such as the deposition rate, temperature, and the chamber pressure. A picture of the microfabricated flow sensor is presented in Fig. 9. It shows PDMS channels with metal deposited on the glass substrate.

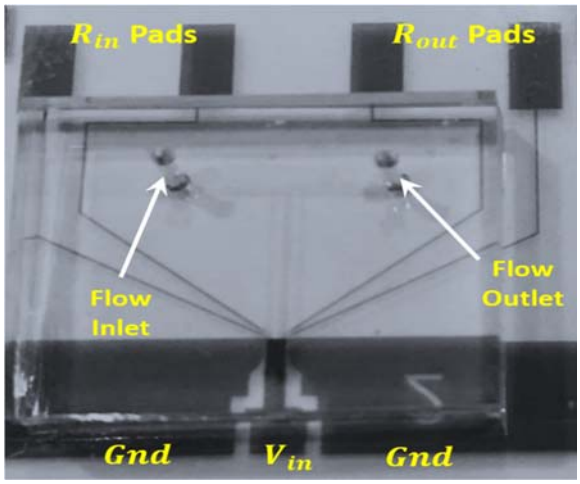

Fig. 9. Microfabricated flow rate sensor. The total device size is 1.5 cm x 1.5 cm.

A microscopic image of the sensing part of the device, including the heating element and the temperature sensors (Microfluidic channels not bonded) is presented in Fig. 10(a).

A zoom-in of the microfabricated microfluidic channel, with a serpentine shape, in contact with the heating element is shown in Fig. 10(b).

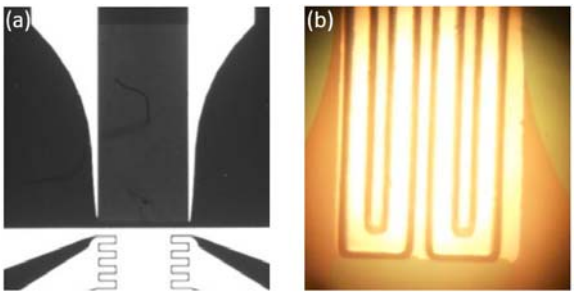

Fig. 10. (a) Microscopic image of the microfabricated sensor; (b) Zoom-in of the fabricated heating element and the microfluidic channels.

5. Experimental Results

5.1. Experiment Setup

Several equipment are used to determine the performance of the fabricated thermal flow rate sensor. The measurement setup is shown in Fig. 11(a).

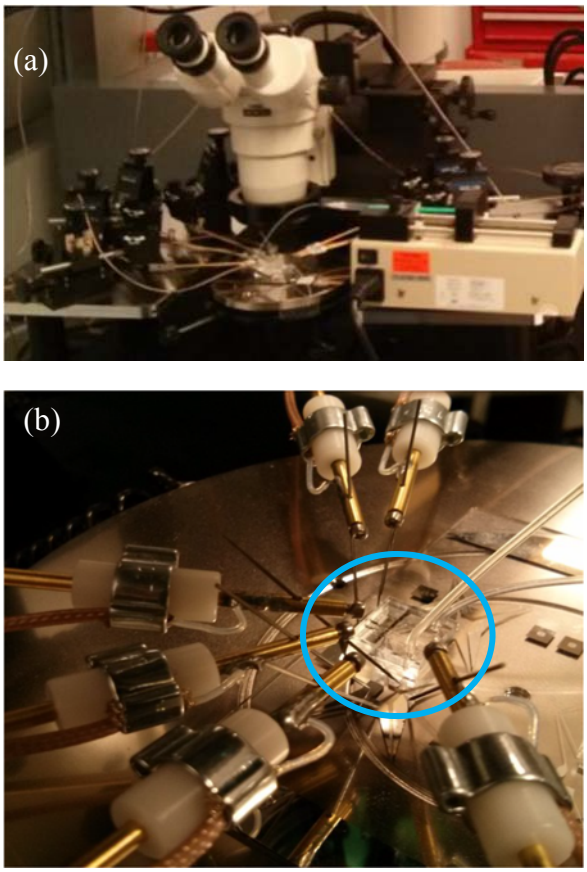

Fig. 11. (a) DC measurement initial setup; (b) Probes setup for DC power measurement.

A "Fisher Scientific" mechanical syringe pump is used to pump the fluid in the micro channel. In addition, a nano volt meter, Agilent 34420A, is used to measure the output voltages of the temperature sensors. A Signatone probe station with six probes and a microscope is used to setup the connections between the device and the other equipment: two probes are used to apply DC power to the heating element, and four probes are used to measure the voltage across the temperature sensors. The applied DC power to the heating element is performed using a Tetronix ps2521 power supply. An applied power to the heating element will generate a heat that is transferred via the fluid to the outlet sensor, resulting in an increase in its resistance. Therefore, the sensor's output voltage increases accordingly. Deionized water is used for the experiment. The microfabricated flow sensor, while being tested on the probe station, is shown inside the blue circle of Fig. 11 (b).

5.2. Sensor Characterization

Several microfabricated devices are used for the characterization of the proposed flow sensor. The calorimetric principle is tested using one of the fabricated devices by measuring the sensor's output voltage V_{out} at a fixed $100\ \mu L/h$ flow rate, and an applied power P_a, the equivalent of an applied voltage, to the heating element. The sensor's response is around $0.9\ mV$ when P_a is $2\ mW$. When increasing the applied power to the heating element, V_{out} increases accordingly as shown in Fig. 12. The sensor's response V_{out} increses to around $0.23\ mV$ at an applied P_a equal to $24\ mW$. It can be noted from the figure that the response time of the sensor while increasing the applied power to the heating element is in the order of 2 to 3 seconds.

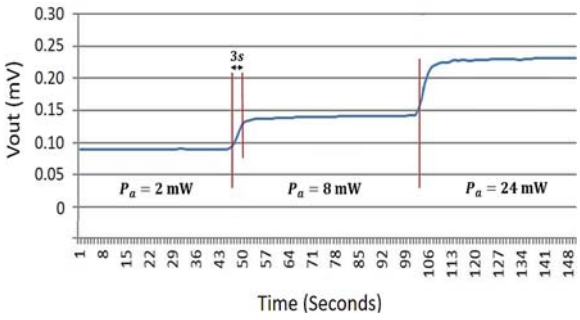

Fig. 12. Temperature sensor output voltage vs. time at different applied powers at the heating element.

The optimization of the device's power consumption is essential in order to increase the battery life time of the complete system. Therefore, it is very important to determine the value of the smallest typical amount of P_a, whithout disturbing the function of the microfabricated device. Therefore, several experiments with different applied power P_a to the heating element are conducted separately to define the typical value of P_a to be used to operate the flow rate sensor.

The blue curve in the chart of Fig. 13 shows the applied voltage to the load over time. It is initially equal to $0\ V$ ($14\ mV$ if considering the offset voltage), $0.05\ V$ in average for the next minute, $0\ V$ for the next second minute, $0.05\ V$ for the next third minute, and $0\ V$ for the rest of the time.

On the other hand, the red curve represents the sensor's output voltage over time function of the applied voltage to the load, either $0\ V$ or $0.05\ V$. Despite the relatively noisy output voltage at each applied voltage to the heating element, it can be noticed that the sensor's output voltage at an applied voltage of $0.05\ V$ can be relatively differentiated from the output voltage when $0\ V$ is applied to the heating element. Whithin the different experiments that are conducted using different applied voltages to the load, $0.05\ V$ applied voltage is considered the typical value that corresponds to the optimum power applied to the

heating element that can operate the fabricated flow rate sensor. That optimum power is around 6 mW.

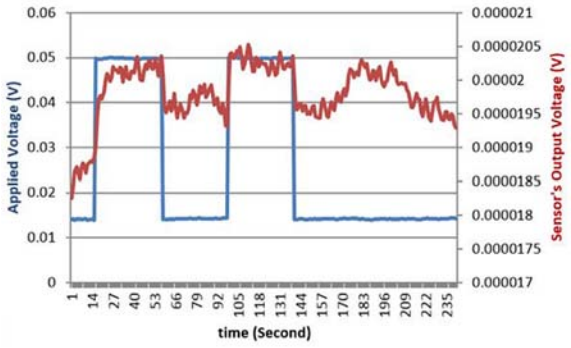

Fig. 13. Temperature sensor output voltage vs. applied voltage to the heating element.

The described experiment is conducted for different microfabricated devices to verify the consistence of the operation. Fig. 14 shows the results summary of two different devices, different from the device used for the results in Fig. 13. The blue diamonds represent the average of sensor's output voltage when no power is applied to the heating element, 0 V, and red squares represent the average of sensor's output voltage when 0.05 V is applied to the heating element. It can be confirmed that there is a noticeable difference between the case where power is applied to the heating element and the case where no power is applied to the heating element, and this confirms the consistency of the device operation for an applied power $P_a = 6\ mW$.

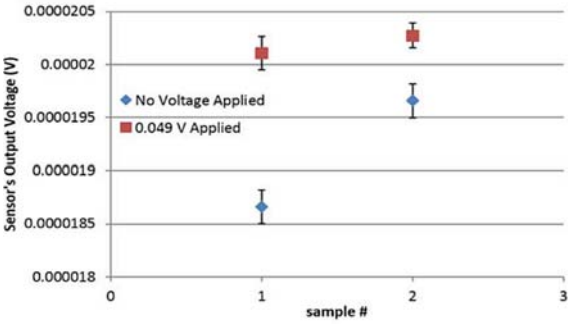

Fig. 14. Temperature sensor output voltage vs. applied voltage to the heating element using two different devices.

A set of microfabricated devices is tested to determine the relationship between the output voltage V_{out} of the temperature sensor at the outlet and the fluid flow rate. It should be noted that each device has to be initially calibrated in order to be used in a complete system. V_{out} Versus the flow rate is presented in the graph of Fig. 15.

Different applied powers to the heating element are experimented: 2.5 mW (black curve), 6 mW (orange curve), and 12 mW (blue curve). It can be concluded that the resolution of the sensor increases as the applied power to the heating element is bigger. Results indicate that at a fixed applied voltage to the heating element, the flow rate increases, while less heat is being transferred to the output temperature sensor, and V_{out} variation is reduced.

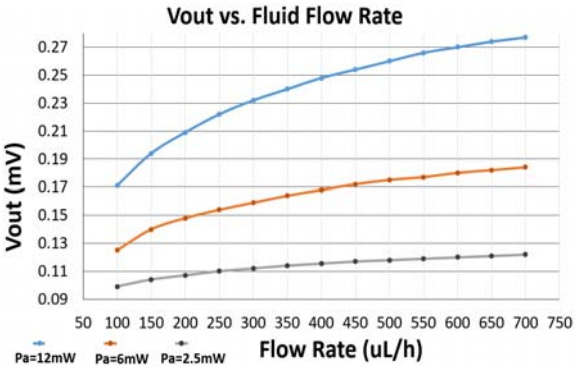

Fig. 15. Outlet temperature sensor voltage vs. fluid flow rate at different applied powers to the heating element.

Fluid flow rate measurement error has been calculated by fixing the fluid pump's flow rate at different values, and then recording flow rate sensor readings over different periods of time. Fig. 16 and Fig. 17 present fluid flow rate sensor readings at fixed 400 µl/h and 500 µl/h, respectively.

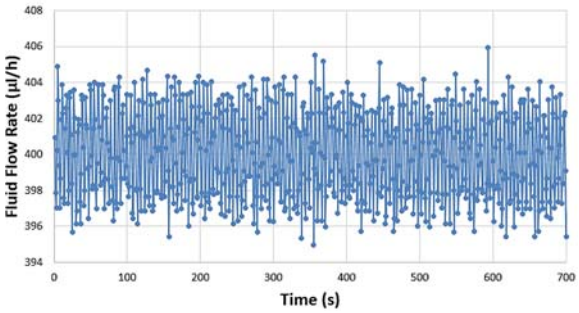

Fig. 16. Measurement of a Fixed 400 µl/h Flow Rate over Time.

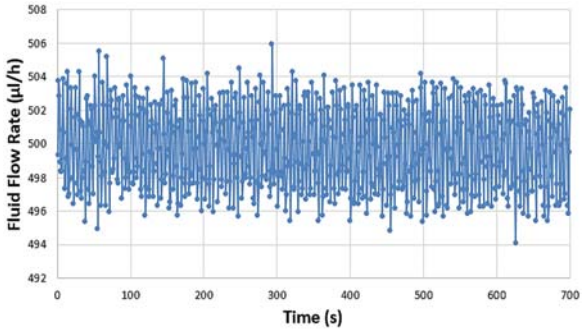

Fig. 17. Measurement of a Fixed 500 µl/h Flow Rate over Time.

Using data recorded over 12 minutes, the average reading error for a fixed flow rate of 400 $\mu l/h$

is $2.16\ \mu l/h$, and the maximum reading error is $5.92\ \mu l/h$. Moreover, the average reading error for a fixed flow rate of $500\ \mu l/h$ is $2.32\ \mu l/h$, and the maximum reading error is $5.9\ \mu l/h$.

5. Conclusions

A calorimetric microfabricated flow rate sensor is demonstrated. Experimental results show that an applied voltage V_{in} to the heating element can generate heat that is transduced into an electrical signal V_{out} to determine the corresponding flow rate of the fluid in use. In the future, the device will be tested in real life biomedical applications. This invasive approach will be much easier to install, use, and manipulate, compared to non-invasive methods such as ultrasound and Doppler measurement [20].

References

[1]. Khan B., Ahmed S., Kakkar V., A Comparative Analysis of Thermal Flow Sensing in Biomedical Applications, *International journal of Biomedical Engineering and Science*, Vol. 3, Issue 3, 2016, pp. 2016-3301.

[2]. Silvestri S., Schena E., Micromachined Flow Sensors in Biomedical Applications, *Micromachines*, 2012, Vol. 3, Issue 2, pp. 225-243.

[3]. Cerimovic S., Keplinger F., Beigelbeck R., Jachimowicz A., Antlinger H., Jakoby B., Monitoring the glycerol concentration in aqueous glycerol solutions using a micromachined flow sensor, in *Proceedings of the Microelectronic Systems Symposium (MESS)*, 2014, pp. 1-6.

[4]. B. Neji, Microfabricated Thermal Flow Rate Sensor, in *Proceedings of the 5th International Conference on Sensors and Electronic Instrumentation Advances (SEIA' 2019)*, Tenerife (Canary Islands), Spain, 25-27 September 2019, pp. 63-68.

[5]. N. T. Nguyen, Micromachined flow sensors - a review, *Flow Measurement and Instrumentation,*Vol. 8, Issue 1, 1997, pp. 7-16.

[6]. J. Collins, A. P. Lee, Microfluidic flow transducer based on the measurement of electrical admittance, *Lab on a Chip*, 2004, Vol. 4, pp. 7-10.

[7]. N. T. Nguyen, S. T. Wereley, Fundamentals and Applications of Microfluidics, *Artech House*, Boston, 2006.

[8]. Z. Yang, R. Maeda, Automatic micro flow rate measurement using a modified computer mouse device, in *Proceedings of the 1st Annual international IEEE-EMBS Special Topic Conference on Microtechnologies in Medicine & Biology*, Lyon, France, 2000.

[9]. T. W. Kuo J., Yu L., Meng E., Micromachined Thermal Flow Sensors - A Review, *Micromachines*, Vol. 3, Issue 3, 2012, pp. 550-573.

[10]. Tyson J., Micro-thermal Flow-rate Detection for Lab on-a-chip Technologies, *Lab on a Chip*, 2018.

[11]. Neji B., Xu J., Titus A. H., Meltzer J., Micro-Fabricated DC Comparison Calorimeter for RF Power Measurement, *Sensors*, Vol. 14, Issue 11, 2014, pp. 20245-20261.

[12]. Shaun F., *et al*., On the co-integration of a thermo-resistive flow-rate sensor in a multi-parameter sensing chip for water network monitoring, in *Proceedings of the 19th International Conference on Solid-State Sensors, Actuators and Microsystems (TRANSDUCERS)*, Kaohsiung, Taiwan, 2017.

[13]. Hayashida Y., *et al*., C208 Development of Micro pressure sensor for applying to MEMS blood-flow meter, in *Proceedings of the JSME Conference on Frontiers in Bioengineering*, Vol. 26, 2015, pp. 145-146.

[14]. Mukouyama Y., *et al.,* PDMS balloon pump with a microfluidic regulator for the continuous drug supply in low flow rate, in *Proceedings of the 28th IEEE International Conference on Micro Electro Mechanical Systems*, Estoril, 2015, pp. 666-669.

[15]. C. M. B. Ho, S. H. Ng, K. H. H. Li, Y. Yoon, 3D printed microfluidics for biological applications, *Lab on a Chip*, Vol. 15, Issue 18, 2015, pp. 3627-3637.

[16]. A. K. Au, W. Huynh, L. F. Horowitz, A. Folch, 3D Printed Microfluidics, *Angew. Chem. Int. Ed*., Vol. 55, Issue 12, 2016, pp. 3862-3681.

[17]. Hamaguchi K., Tsuchiyama T., Matsushita J., Oxidation of Tantalum Nitride, *Materials Science Forum*, Vol. 761, 2013, pp. 125-129.

[18]. T. Chen, *et al*., Physical and optical properties of ZnO thin films grown by DC sputtering deposition, in *Proceedings of the 9th International Conference on Solid State and Integrated Circuit Technology*, Oct. 2008, 742-745.

[19]. M. H. S. Alrashdan, *et al*., Aluminum nitride thin film deposition using DC sputtering, in *Proceedings of the IEEE International Conference on Semiconductor Electronics*, Aug. 2014. 72-75.

[20]. Ma L., Liu J., Wang J., Study of the Accuracy of Ultrasonic Flowmeters for Liquid, *AASRI Procedia*, Vol. 3, 2012, pp. 14-20.